Final Draft
of the original manuscript:

Stanev, E.V.; Grayek, S.; Staneva, J.:
Temporal and spatial circulation patterns in the East Frisian Wadden Sea
In: Ocean Dynamics (2008) Springer

DOI: 10.1007/s10236-008-0159-0

Temporal and Spatial Circulation Patterns in the East Frisian Wadden Sea

Emil V. Stanev[1,2], Sebastian Grayek[2], and Joanna Staneva[1]

1: Institute for Coastal Research, GKSS Research Centre, Max-Planck-Strasse 1, 21502 Geesthacht, Germany

2: Institute for Chemistry and Biology of the Sea, University of Oldenburg, Carl-von-Ossietzky-Strasse 9-11, D-26111 Oldenburg, Germany

Submitted to Ocean Dynamics, WATT Special Issue (May 2008)

Keywords: Tidal Basins, Statistical Characteristics, Predictability of Circulation

Abstract

This work deals with the analysis of simulations carried out with a primitive equation numerical model for the region of the East Frisian Wadden Sea. The model with 200 m resolution is forced by wind, air-sea heat and water fluxes and river runoff and is nested in the German Bight 1 km-resolution numerical model. The question addressed in this paper is how well the model output can be compressed with the help of EOF analysis. It is demonstrated that for the short-time periods of the order of spring-neap cycle, only several modes are enough to almost fully represent the circulation. This is just an illustration that circulation in this region is subject to dominating tidal forcing creating clear and relatively simple response patterns. However, for longer periods of about several months, wind forcing takes over and the circulation patterns become much more complex. Possible application of the results in hindcasting and forecasting of hydrodynamics and sediment dynamics in the coastal zone is considered.

1 Introduction

Numerous evidences of the response of the coastal ocean to tides exist based on local observations, e. g. tidal gauge data. However, spatial patterns are much less clear because direct observations over large areas and with high spatial resolution are limited. Remote sensing data also do not help much: altimeter data are not precise enough in the near coastal zone, ocean color or AVHRR data are affected by cloud conditions and do not provide complete information with sufficient temporal resolution. In the East Frisian Wadden Sea, which is the area of our research interest, the temporal and spatial variability derived from statistical analyses of outputs from numerical models is not enough explored, although some initial steps have already been made (Stanev et al., 2006a).

The work presented here has been carried out within the framework of the research programme "BioGeoChemistry of Tidal Flats", which combines various research activities aiming to improve the basic understanding of functioning of these areas, including circulation and sediment transport (Staneva et al., 2008). Our major aim here is to make an initial effort towards developing techniques enabling the best use of data for state estimates and forecasting purposes. One necessary step, before going deeper into this issue and before addressing data assimilation is to understand the dominating statistical properties of coastal dynamics.

The German Bight (Fig. 1a), which is bordered by the coasts of the Netherlands, Germany, and Denmark, is situated in the south-eastern corner of the North Sea. It is well established that the wind in this area results in a cyclonic residual circulation, i.e. a circulation in the direction of propagation of the tidal wave (from west to east along the southern boundary and from south to north along the western coasts of Germany and Denmark).

The East-Frisian Wadden Sea (Fig. 1b) is one of the shallowest areas of the German Bight, being characterized by a series of barrier islands, each 5-10 km long in the east-west direction and 2-3 km wide (Fig. 1b). The tidal range varies from $\sim$ 2.5 m (Isles of Borkum and Sylt) to $\sim$ 3.5 m (the Elbe Estuary), i.e. the region is exposed to upper meso-tidal conditions.

Wadden Sea water periodically mixes with North Sea waters (during flood), and is partially exported into the North Sea (during ebb). In this way, the Wadden Sea acts as a buffer mixing-zone between ocean and land. The exchange of water and properties between the Wadden Sea and the German Bight are known from numerical simulations (Stanev et al., 2003a,b; Stanev et al., 2006a) and numerous observations (see this Special Issue).

It is well-known that one fundamental characteristic of the East-Frisian Wadden Sea is the vigorous suspended matter dynamics (Santamarina Cuneo and Flemming, 2000; Burchard

at al., 2008) triggered by the turbulence due to velocity shear (Stanev et al., 2007) and wind waves (Gayer at al., 2006; Stanev et al., 2006b). Understanding sediment dynamics is thus crucially dependent upon the knowledge on the turbulence regime. Therefore specific attention in this paper is also payed to the question of how complex the turbulence patterns are in the region of the East Frisian Wadden Sea.

Detailed validation of numerical models against observations at fixed locations (Stanev et al. 2003a, 2006a), and over larger areas (Staneva et al., 2008) demonstrates a good quality of numerical simulations and motivates us to address the question: what are the dominating temporal and spatial patterns? Provided that the latter show some robustness, we could hope that it would not be too difficult to extend this research towards the issue about predictability, which has never been addressed for this region.

The paper is structured as follows: we first describe in Section 2 the numerical model and setup, followed by a description of the simulated spatial and temporal patterns in Section 3. Statistical reconstruction of simulations is presented in Section 4. The paper ends with brief conclusions.

2 Numerical model

The model system used here consists of two models with different horizontal resolution: German Bight Model (GBM) and Wadden Sea Model. Both models are based on the 3-D primitive equation numerical model (Burchard and Bolding, 2002), in which the equations for the three velocity components u, v and w, sea-surface height (SSH) ζ, temperature T, salinity S, as well as the equations for turbulent kinetic energy (TKE) and the eddy dissipation rate due to viscosity are solved. The models use terrain-following equidistant vertical coordinates (σ-coordinates) and are capable to simulate drying and flooding of tidal flats. The vertical column is discretized into ten non-intersecting layers. The application of the models to the area of our study is described by Stanev et al. (2006a) and Staneva et al., (2008) and we refer to these papers for more details.

The Wadden Sea model with a resolution of 200 m is nested in a German Bight Model with resolution of about 1 km (Staneva et al., 2008). The horizontal discretization of both models is done on a spherical grid. The atmospheric forcing for both models is computed trough bulk aerodynamic formulas using 6-hourly ECMWF re-analyses data. Below we briefly formulate the differences in the forcing of two models.

For the outer mode (GBM) the river run-off for the rivers Elbe, Ems and Wesser is taken from the 1-hourly data provided by the Bundesamtes für Seeschifffahrt und Hydrographie

(BSH). The lateral boundary conditions of sea surface elevations, salinity and temperature are taken from the operational BSH model (Dick and Sötje 1990; Dick et al. 2001).
For the inner (Wadden Sea) model the forcing at the open boundaries is taken from the simulations with the GBM (Staneva et al., 2008) and interpolated in time and space onto the grid points along the boundaries of the Wadden Sea regional model. The nesting is done one-way, i.e. the nested model receives boundary values from the coarser model but does not influence the coarser resolution model. The fresh-water fluxes from the main tributaries in the region are taken from the observations compiled in an internal report of the Niedersächsischer Landesbetrieb für Wasserwirtschaft, Küsten- und Naturschutz, Aurich, Germany.
The present study analyses numerical simulations carried out for the period September-December 2006. This four-months period is long enough to resolve the major dominating temporal scales associated with tidal (flood-ebb, spring-neap) and atmospheric (synoptic) forcing. Unlike the past studies based on the same model, the present one addresses also the response to extreme events. One such event was the storm surge Britta on 1. November 2006. This event extended over the entire North Sea (Fig. 2a, b), atmospheric pressure was below 984 hPa, and extreme values of sea level (Fig. 2c) were reached in many continental locations (e. g. Emden 3,59 m above the mean high water) as well as at barrier islands (Langeoog und Wangerooge). This storm surge belongs to the strongest ones observed in the last 100 years along the Lower Saxony coast. The reason for extremely high water was the long duration of strong northwest wind (up to 156 km/hour) working in parallel with tides. The maximum observed wind speeds on most barrier islands were above 125 km/hour (the estimates based on ECMWF reanalysis data, Fig. 3 give slightly lower values).
The results from simulations are described in more detail by (Staneva et al., 2008). In the present paper, we focus on the circulation. Presentation of performance of the model in simulating temperature and salinity is provided in the earlier publication. The present simulations (Fig. 4) are in overall consistency with the earlier ones, in particular, as it concerns the transport through the straits. The general pattern is characterized by extreme velocities in the tidal inlets, westward currents in front of the barrier islands during ebb, and eastward currents during flood.
Extremely stormy weather during some periods enabled us to analyze the response of the model in very special conditions. Although Fig. 4b and Fig. 4d correspond to the same tidal phases (short after flood starts, that is short after low water) during two consequent neap-spring tidal periods, Wadden Sea almost does not get dry during the first period (storm

Britta). It is also noteworthy much higher ebb velocity during storm Britta (compare Fig. 4a and Fig. 4c), in particular on tidal flats. The comparison with observations (Fig. 5) demonstrates that the model replicates sufficiently well the major sea-level variability in the area of our simulations.

3 EOF-analysis of simulations

3.1 Temporal variability

Statistical decomposition of the time-space signals with the help of the empirical orthogonal function (EOF) analysis facilitates the understanding of the most important spatial patterns and their temporal evolution (see e. g. von Storch and Zwiers 1999). The latter are usually called principle components (PC). Sometimes a direct link can be seen between the spatial (EOF) and PC patterns from one side, and physical processes, from another, which is not theoretically justified by the method. However, we will demonstrate that in our particular case, as in many other ones, most of the statistical information has high level of physical consistence (see also Stanev et al., 2006a).

The overall behavior of dynamics can be better understood if we analyze the most complete dataset, therefore, we do not process each individual field one by one, but take sea level and two velocity components as one state vector. The advantage of this approach is that it is coherent with procedures used in some data assimilation techniques. The disadvantage is that it might not clearly display some major physical characteristics of individual fields. To simplify the analysis and to avoid transformations from sigma into z-coordinate system we analyze surface and bottom properties only.

From the whole period September-December we chose two periods, which are characterized by calm weather (18 September 2006 - 02 October 2006, referred further as "calm") and weather dominated by strong winds (01-14 December 2006, referred further as "windy", see Fig. 3). For these periods we process the model data sampled with 60 min resolution. Furthermore, to ensure homogeneous datasets in "calm" and "windy" we exclude from analysis locations which fall dry.

Another analysis has been performed on the signal from which tidal variability with frequency higher than diurnal was filtered out. The corresponding analysis is referred to as "no-tidal", although it contains, along with the synoptic variability, longer-term variability associated with spring-neap tidal cycle.

The percentage of variance explained by the first three oscillation modes in "calm" and "windy" cases (Table 1) demonstrates that the tidal signal (see also Fig. 6) is the strongest

Table 1: Percentage of variance explained by the first three EOF-s.

mode	calm		windy	
no	dynamics	TKE	dynamics	TKE
1	82.7	86.3	83.1	85.4
2	16.7	6.7	16.3	6.8
3	0.2	2.7	0.2	2.8
sum	99.6	95.7	99.6	95.0

one. Because the response of the shallow Wadden Sea to tidal forcing is relatively simple (Stanev et al., 2003a, b), a very limited number of modes describes well the total variance. Comparison between PC-1 (Fig. 6a) and analyzed fields demonstrates that this component almost repeats the tidal oscillations of the sea level. PC-2 shows a phase shift of about a quarter tidal period relative to PC-1 and corresponds to velocity oscillations. This curve represents semidiurnal tidal oscillations modulated by spring-neap periodicity. The well known asymmetry associated with the non-linear response of tidal flats (Stanev et al., 2003a) is seen in this signal: different times are needed to establish maximum flood or maximum ebb velocity (Fig. 7). In particular, longer time is needed for the currents to evolve from maximum ebb to maximin flood, than for the inverse transformation (note that negative PC-2 corresponds to flood). This does not only support the above mentioned theoretical results, which have been mostly applied to tidal channels, but also demonstrates that the so called "ebb-dominance", or according to the terminology of Friedrichs and Madsen (1992) "shorter-falling asymmetry" dominates the tidal response in this region as a whole.

PC-3 (Fig. 6c) represents $\sim$ 6 hourly periodicity, which is associated with the maximum in current magnitude (twice per tidal period).This type of variability reminds the similar type of variability detected in observations (Stanev et al., 2006a), namely the two maxima are different (the one during flood is higher, see Fig. 7).

The major characteristics of principle components of TKE is the semi-tidal periodicity (about 6 hour), which is pronouncedly modulated by the spring-neap signal (Fig. 8). This is just an illustration that the level of TKE in the Wadden Sea is very sensitive to

this important astronomical forcing. The second important characteristic of turbulence is the strong difference in the PC maxima during flood and ebb. This gives a clear support of earlier theories about asymmetric responses (Stanev et al., 2006a), which are enhanced during spring-tide. Comparison between the PC-1 of TKE and the sea level curve (not shown here) demonstrates clearly that maximum amplitudes in TKE are reached by high water during spring tide. This result could give an indication that during this part of tidal period resuspended and eroded from bottom sediment (here, we assume that concentrations are expected to reach higher values if turbulence is stronger) is transported towards land. This could provide an explanation about why tidal flats tend to accumulate sediment.

Comparison between the principle components during calm and windy weather shows that no remarkable differences can be identified (see also Table 1). This supports the idea that in the Wadden Sea, tidal response is dominating, therefore, the corresponding curves from "windy" period are not shown here. However, the model output from which the tidal signal has been filtered out gives quite a different view on the temporal variability (Fig. 9). In this data set the first three EOF-s describe 76.3, 11.0, and 5.6 percent of the total variance (97.9 percent in total). PC-1 shows some correlation both with the course of SSH forcing (dashed red line in Fig. 9a) for some of extreme events and wind magnitude (dashed blue line in Fig. 9a) for longer-term variability. PC-2 is dominated by extreme events (storm surge Britta), while PC-3 is modulated by spring-neap oscillations, in particularly for the more calm first part of analyzed period (see Fif. 3).

3.2 Horizontal Patterns

The first EOF in "calm" (Fig. 10a) is positive throughout the model area. This oscillation mode displays the up-and-down motion of the sea level caused by tides, which is unidirectional over the entire area. The east-west gradient gives an illustration of the known fact that the tidal range in this region increases from west to east. Tidal channels show a tidal range as high as the adjacent open-ocean areas north of them.

A parallel analysis of the entire data including data in the regions getting dry has also been done (results are not shown here). Because sea level is "frozen" in the model when the water column thickness reaches the minimum allowable value of 2 cm data series are not homogeneous. Nevertheless, the two analyses demonstrate no big differences in the deep regions. In the regions undergoing drying and flooding EOF-1 of the sea level follows the bottom topography (smallest variability in areas remaining dry for longer times), and as it was the case of deep data only, has the same sign throughout the model area.

EOF-2 (Fig. 10b) shows an east-west propagation pattern and gives a measure of the phase difference between channels and the areas north of the barrier islands. The delay is approximately equal to the time needed for tidal wave to cover the distance of about one barrier-island length (notice that we observe same colors, green in this case, in front of Spiekeroog and behind Langeoog Islands).

From the horizontal pattern of EOF-3 it seems plausible that this mode corresponds to another known physical process, that is the east-west asymmetry of 6-hour variability, which is enhanced during flood. Notice that, in this case the response of the tidal channels is coherent with the processes north of the tidal inlets. Furthermore, bearing in mind that (1) this variability pattern is dominated by 6-hour oscillations and (2) that the analysis of the entire data set (deep area and area undergoing drying) shows inverse trends in the deep part and over the tidal flats, one could also conclude that this signal is indicative for the transformation of tidal response in the Wadden Sea in a way that the $\sim$ 6-hourly variability is coherent over the entire region of tidal flats (see also Stanev et al., 2003a).

EOF-1 of u-velocity (Fig. 11a) displays an inverse correlation between the variability in tidal channels and the shallow area adjacent to the northern coasts of barrier islands (the north-west tips of the barrier islands give the "origin" of the inverse to the tidal channels signal). Furthermore, negative correlation is also observed between the area along the northern model boundary and the shallows north of the barrier islands. The latter structure is indicative for the rotational character of tidal excursions north of the barrier-islands. This type of oscillation is coherent with the up-and-down motion of sea level (see Fig. 6).

The EOF-1 of v-velocity (Fig. 11b) shows a pronounced anti-correlation between tidal channels and the areas in the middle north and south (in the second case this is revealed by the analysis of data containing information about tidal flats) of barrier islands. It is noteworthy that this "rule" is more applicable to the eastern tidal channels, which is just a consequence of the larger tidal range in the eastern part.

EOF-2 of velocity (Fig. 11c, d) displays some important characteristics of the dynamics of tidal channels. The inverse correlation (in particular in u-EOF-2) enables us to identify the split of channels as flood and ebb ones, which is also known from observations (Stanev et al., 2006a). The transformation of the v-signal along tidal channels (maxima and minima in Fig. 11d) gives a clear support of the theory (Stanev et al., 2007b) that tidal channels in the East Frisian Wadden Sea evolve from ebb-dominated (between barrier islands) to flood dominated (in their shallowest extensions).

North of the barrier islands, an eastward "protrusion" of v-EOF-2 pattern is clearly seen,

which is indicative of the export patterns from the tidal flats (from the western island to the eastern one). The horizontal patterns of the 6-hour variability (see Fig. 6c) which is mostly associated with currents magnitude show quite different patterns for the two velocity components (Fig. 11e, f). While for the meridional transport the maximum variability is limited to the narrow area between neighboring islands (Fig. 11f) maximum variability of zonal transport is observed in the zonal part of channels, which can easily be expected. However, what is not so trivial is the inverse correlation between u-patterns in different zonal sections of channels indicating complicated evolution of the tidal responses. The horizontal patterns of TKE could give an indirect information about the location of areas favorable to deposition and erosion. EOF-1 pattern, which is a unidirectional variability over the entire area (Fig. 12a) demonstrates clearly large differences in the magnitudes of oscillations in tidal channels and flat areas in front and behind the barrier islands. In addition to the well known asymmetries explaining tendencies of erosion and deposition in the Wadden Sea (Groen, 1967; Postma, 1982; Stanev et al., 2003b; Stanev et al., 2006a), we see in the TKE-EOF-1 pattern a rather complicated spatial structure with different magnitudes in deep parts of channels and their northern extensions, from one side and in the remaining areas, from the other.

EOF-2 of TKE seems easier to be interpreted. This variability is strongly dominated by the neap-spring cycle, enhancing velocity magnitude along the channels (Fig. 12b). Eastern and westernmost areas of the open sea are inversely correlated, which demonstrates the sensitivity of TKE patterns to different tidal ranges in these zones. As for the TKE-EOF-3 (a very low-magnitude signal), the major horizontal characteristic are the opposing trends occurring in the channels north and south of the straits.

The analysis of temporal and spatial variability in no-tide case is focused on transport characteristics because they do give the most clear illustration of responce to extreme events. With respect to the sea-level characteristics we will only mention that the responce is relatively simple, as can be seen from Fig. 4, displaying a uniform in north-south direction field. The EOF-1 (not shown here) shows a unidirectional change throughout the area, which amplifies in the south-eastern corner of the German Bight (easternmost extension of our model area). EOF-2 (also not shown here), which is related to periodic intensification with neap-spring periodicity is well structured in the tidal channels.

EOF-1 of zonal velocity component (Fig. 13a) has the same sign throughout most of the area. This could be explained by the adjustment of zonal circulation to winds with dominating zonal component. The strongest response (largest values of EOF-1) is observed in the open sea, which decreases with decreasing distance from the barrier islands. In the

tidal flats, the horizontal contract in the amplitudes of oscillation is very small, except for a small area south of Norderney Island.
The EOF-1 and EOF-2 patterns of bottom velocity (not shown here) are similar to the ones in Fig. 13a, b revealing that in this area there is not substantial change of dynamics with respect to the vertical coordinate.
Another interesting difference from tidal cases is observed in the no-tidal one: the zonal motion north of the islands "displays" some undulated patterns, which well coincide with irregularities in the bottom relief. This EOF-structure is not observed in the case of tidal response.
In EOF-1 of meridional velocity (Fig. 13b) some pronounced differenced from "calm" are obvious: meridional transport in channels Otzum and Accum is split into two: south-east of the strait, the correlation is positive with the oscillations at the coast of western island. In this way, a *quadropul-like pattern* is formed, which is characteristic for the regime of a two-way transport in the straits driven by wind.
EOF-2 corresponding to longer-term variability of zonal velocity (Fig. 13c) is completely different from the one in the case of tidal forcing. The pattern north of the barrier islands (alternating positive and negative correlations) could indicate divergence and convergence in this component. As a whole, tidal flats and the areas north of the barrier islands are negatively correlated.
The propagation pattern associated with EOF-2 of meridional transport (Fig. 13d) is relatively simple and clear: the area north of straits is well defined and usually negatively correlated with the variability in most parts of the remaining area. This result gives an idea about how the response to extreme events (storm Britta in this case) is horizontally structured.
The two EOF-3 (Fig. 13e, f) reveal the response-patterns to neap-spring cycle (see Fig. 9). Although this is a relatively week signal compared to the one originating from extreme events it is very well structured. The zonal component reflects inverse correlation between western and central regions north of barrier islands, while meridional component pattern is "divided" in two north of inlets. This illustrates that evolution triggered by neap-spring cycle might affect transport in the area of tidal deltas.

4 Statistical reconstructions

Provided that major processes could be well described by several EOF-s only, one might want to ask the question about the quality of statistical reconstruction and forecast. In

order to address this issue, we use simulations during "calm" and "windy". Then using twelve modes only, we reconstruct the simulations. Comparison between real (model output) and synthetic (reconstructed using limited amount of EOF-s) data demonstrates that mean error is about 0.03 sigma for sea level and 0.12 and 0.19 sigma for u and v, correspondingly. These are very small errors.

Motivated by the above results we go one step further and ask the question: could a reconstruction (forecast) be done based on a limited amount of input information. This is a relevant question for the project, in the frame of which this research has been carried out. In the Otzumer Balje (see Fig. 1b for the location) a continuously operating data station has been deployed (Staneva et al., 2008). The measured data (sea level temperature, salinity and velocity at several levels) are available online and the use of these data for forecast purposes seems challenging. In the past years, a similar data station operated by the GKSS Research Centre was deployed in the Accumer Ee (square in the Accumer Ee, Fig. 1b). The second question is: would it be possible using data from both stations to increase the quality of reconstructions, compared to the case of only one station statistical forecast.

Leaded by the above two questions, we take the model data only in the positions of data stations and construct by multivariate EOF-analyses of extracted variables the PCs of "observations" (synthetic observations) for both periods (PC_{oc} and PC_{ow}. Indices "o", "c" and "w" stay for "observations", "calm" and "windy", correspondingly. For the forecast based on one data station (sea level and two velocity components at sea surface and bottom) we are able to calculate at most five PC-s; for the forecast based on two data stations, ten PC-s can be derived. We use the same amount of global domain PC-s from the calm period (PC_{gc}) to train the forecast. Therefore we apply a linear regression on PC_{oc} and PC_{gc} and obtain a set of linear parameters (L_c) to convert PCs of observations into PCs of global domain. Finally, the forecast of windy period ($Forc_w$) is calculated by:

$$Forc_w = EOF_c \cdot L_c \cdot PC_{ow} \tag{1}$$

For comparison, we also calculate a reconstruction of windy period ($Reco_w$) from the first twelve EOFs and PCs of windy period by:

$$Reco_w = EOF_w \cdot PC_w \tag{2}$$

The root mean square forecast and reconstruction errors are calculated at each grid and are shown as maps of percentage of standard deviation. In the heading of each plot, are

shown the area mean values of errors of reconstruction, forecast using one data station, and forecast using two data stations. Obviously, the statistical forecast is worse than the reconstruction, however, taking into consideration the usual errors in observations, the results are encouraging.

Something unexpected from our reconstructions deserves to be mentioned here. The initial expectation was that adding one more data station would substantially increase the accuracy of forecast. This, however appeared not to be the case because the two data stations are very well correlated (see results in Section 3). Actually, not much new information is added by adding data from the second station. Additional reconstructions and forecasts based on different positions of data stations (not shown here) prove that some improvement is still possible by optimizing the deployment of stations.

5 Conclusions

This paper presents a statistical analysis of model simulation, which could be considered as a first step towards data assimilation of continuous observations in the Wadden Sea. Some of the results support in a more objective way earlier ones based on more limited analyses. In particular, temporal asymmetries due to specific hypsometric properties of tidal basins, evolution of tidal signals along channels from ebb dominated between the barrier islands to flood dominated in their shallow extensions are well captured by the statistical analyses. It has been shown that, without losing much detail, the information about circulation is easily "compressible" to several modes only. This enables correct reconstructions and statistical forecasts using local measurements only. This could appear as a good tool for simple and rapid estimates of the sea state using the observations on continuously operating data stations. Our belief is that the results presented are relevant to other similar cases of coastal dynamics and could motivate wider application of the techniques used here beyond the currently studied area.

ACKNOWLEDGMENTS

We acknowledge the support of the research programme "BioGeoChemistry of Tidal Flats", and the EC-funded IP ECOOP.

References

[1] Burchard H., K. Bolding, 2002. GETM - a General Estuarine Transport Model. Scientific Documentation, No EUR 20253 EN, European Commission, printed in Italy, 157 pp.

[2] Burchard, H., G. Flser, J. V. Staneva, T. H. Badewien, and R. Riethmueller, 2008. Impact of density gradients on net sediment transport into the Wadden Sea, Journal of Physical Oceanography, Vol. 38, 3, 566-587.

[3] Dick SK, Eckhard K, Müller-Navarra SH, Klein H, Komo H (2001) The operational circulation model of BSH (BSHcmod)- Model description and validation. Berichte des Bundesamtes füSeeschifffahrt und Hydrographie (BSH): 29, 49pp

[4] Dick SK, Sötje K (1990) Ein operationelles Ölausbreitungsmodell für die deutsche Bucht. Dt Hydrogr Zeitschrift, Ergänzungsheft Reihe A 16: 243-254

[5] Dyer K.R. R.L. Soulsby, 1988. Sand transport on the continental shelf. Annual Review of Fluid Mechanics 20: 295-324.

[6] Flemming B.W., 2004. Factors affecting the shape of particle frequency distribution and associated textural parameters. In: From particle size to sediment dynamics, edited by B W Flemming, 53-58.

[7] Friedrichs, C.T., & Madsen, O.S., Nonlinear diffusion of the tidal signal in frictionally dominated embayments, 1992, J. Geophys. Res., 97, 5637-5650.

[8] Gayer, G, S. Dick, 2006. Numerical modeling of suspended matter transport in the North Sea Ocean dynamics 56(1), 62-77.

[9] Groen, P. (1967) On the residual transport of suspended matter by an alternating tidal current, Netherlands Journal of Sea Research 3 (1967), pp. 564574

[10] Pleskaschevski A., G. Gayer, J. Horstmann, W. Rosenthal, 2005. Synergy of Satellite Remote Sensing and Numerical Modeling for Monitoring of Suspended Particulate Matter. Ocean Dynamics, DOI 10.1007/s10236-004-0101-z, Vol. 55(1), pp. 2-9.

[11] Postma, H. (1982) Hydrography of the Wadden sea: movements and properties of water and particulate matter. In: Postma, H. (Ed.), Final Report on Hydrography of the Wadden Sea Working GroupReport 2, Rotterdam, Balkema, 76pp.

[12] Santamarina Cuneo P., B. Flemming, 2000. Quantifying the concentration and flux of suspended particulate matter through a tidal inlet of the East Frisian Wadden Sea by acoustic Doppler current profiling. In: Flemming, B.W., Delafontaine, M.T., Liebezeit, G. (Eds.) Muddy Coast Dynamics and Resource Management, Elsevier Science, Amsterdam, The Netherlands, pp 39-52.

[13] Stanev E.V., G. Brink-Spalink, and J.-O. Wolff (2007), Sediment dynamics in tidally dominated environments controlled by transport and turbulence: A case study for the East Frisian Wadden Sea, J. Geophys. Res., 112, C04018, doi:10.1029/2005JC003045.

[14] Stanev, E. V., B. Flemming, A. Bartholomae, J. Staneva, and J.-O. Wolff (2006a) Vertical circulation in shallow tidal inlets and back barrier basins. Continental Shelf Research, v. 27, iss. 6, p. 798-831.

[15] Stanev E.V., G. Flöser, J.-O. Wolff, 2003a. Dynamical control on water exchanges between tidal basins and the open ocean. A Case Study for the East Frisian Wadden Sea. Ocean Dynamics, 53, 146-165.

[16] Stanev, E. V., J. O. Wolff, and G. Brink-Spalink (2006b) On the sensitivity of sedimentary system in the East Frisian Wadden Sea to sea level rise and magnitude of wind waves. Ocean Dynamics 56(3-4): 266-283

[17] Stanev E.V., J.-O. Wolff, H. Burchard, K. Bolding, G. Flöser, 2003b. On the Circulation in the East Frisian Wadden Sea: Numerical modeling and data analysis. Ocean Dynamics, 53, 27-51.

[18] Staneva J., K. Bolding, A. Stips, 2007 A nested grid model for studying the German Bight circulation. Ocean Dynamics, (in preparation)

[19] Staneva, J., Stanev, E. V., Wolff, J.-O., Badewien, T. H., Reuter, R., Flemming, B., Bartholoma, A., and K. Bolding (2008) Hydrodynamics and Sediment Dynamics in the German Bight. A Focus on Observations and Numerical Modelling in the East Frisian Wadden Sea, Cont. Sh. Res. (in press)

6 Figures

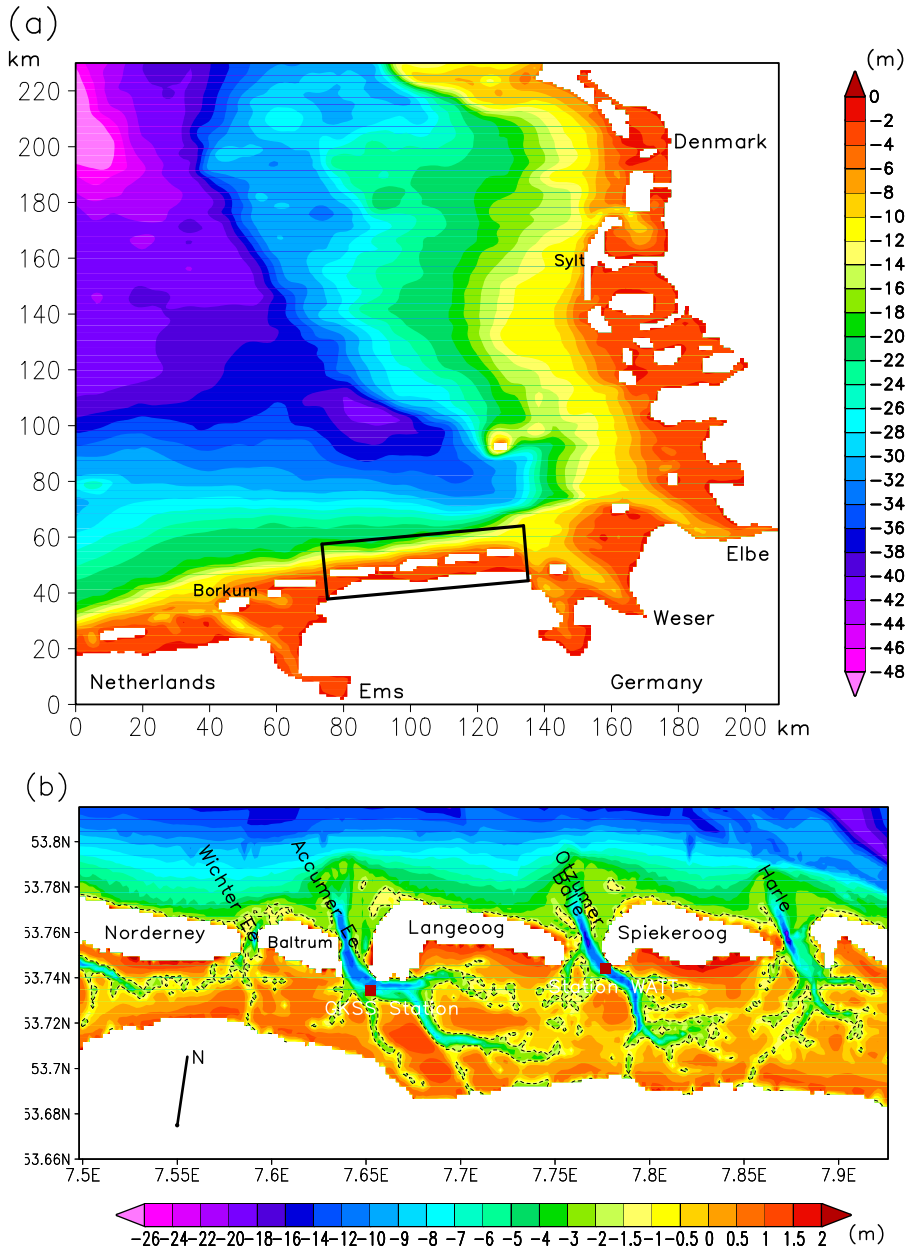

Figure 1: Topography of the German Bight (a) and East Frisian Wadden Sea (b). Dashed line in (b) contours regions, which are subject to drying. The position of continuously operating data stations are given with red squares.

a)

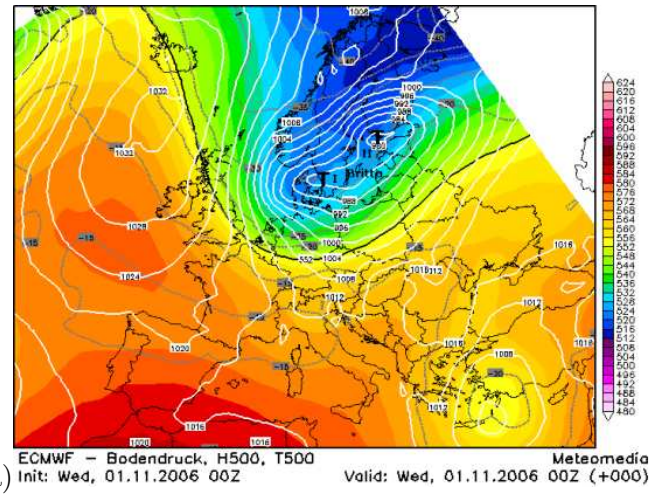

b)

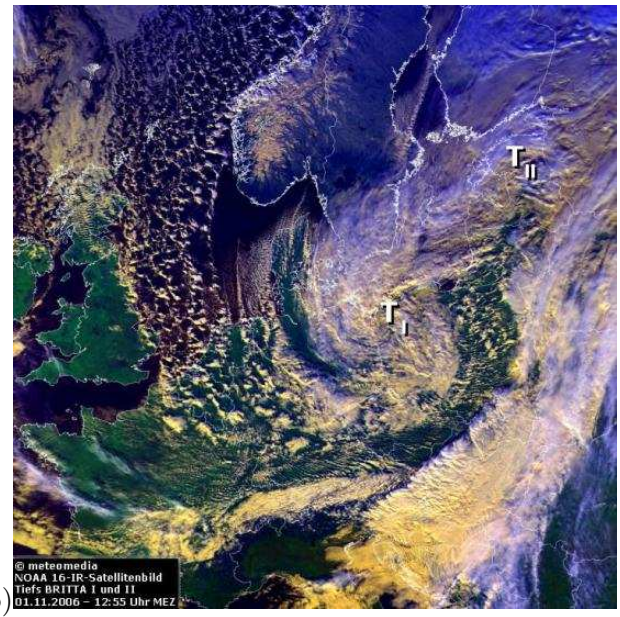

c)

Figure 2: Surface pressure (a), satellite image (b) and visual observation (c) during storm surge Britta. Courtesy: ECMWF, NOAA and NLWKN (Niedersächsischer Landesbetrieb für Wasserwirtschaft, Küsten- und Naturschutz), Aurich, Germany.

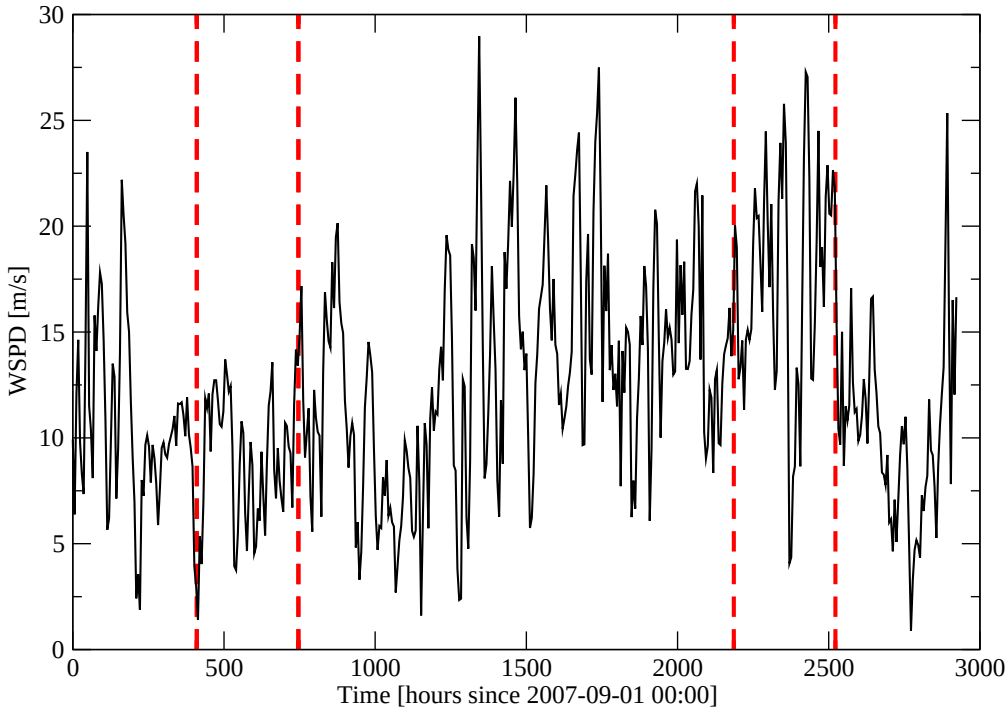

Figure 3: Mean wind magnitude in the model region during the period of simulations based on ECMWF reanalysis data. The vertical dashed lines display the two analysis periods, "calm" and "windy".

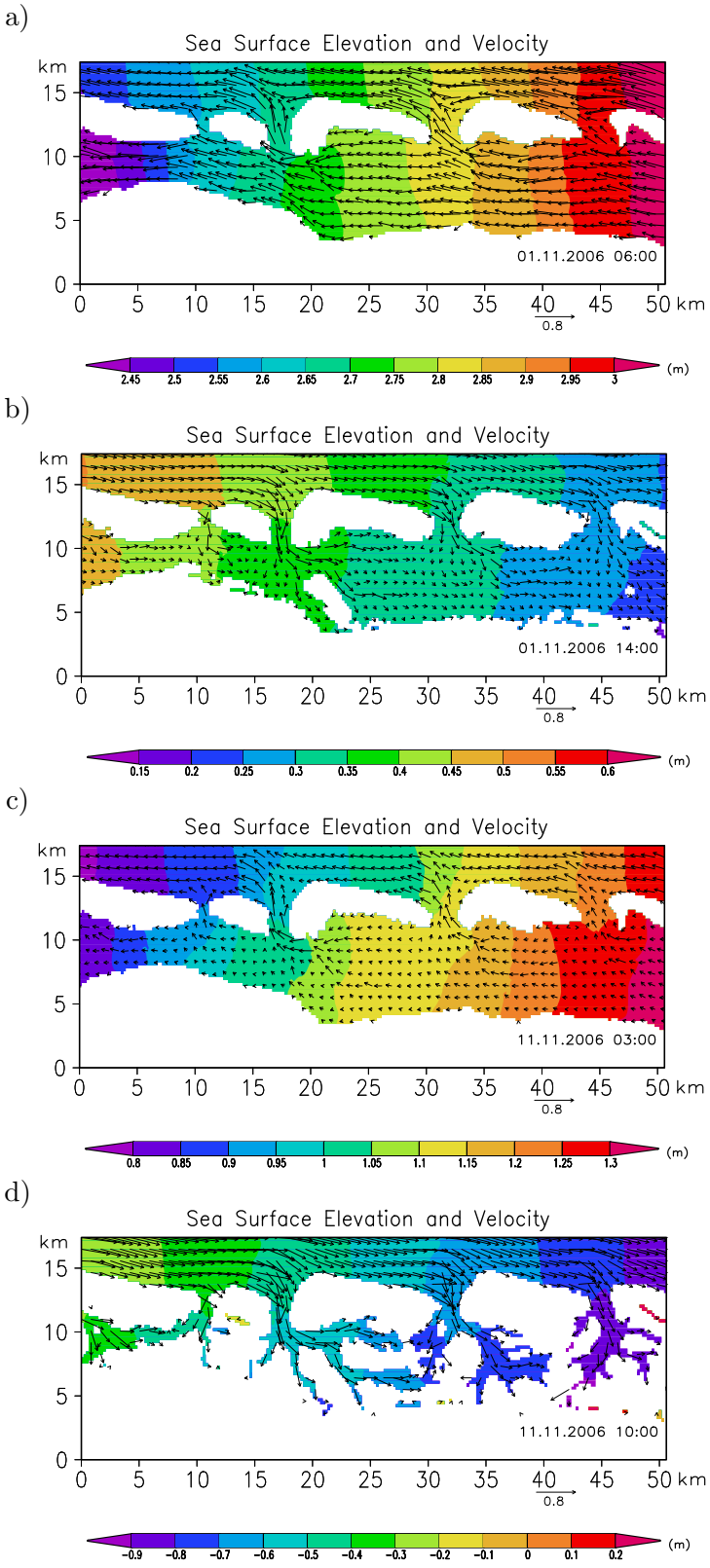

Figure 4: Simulated velocities during ebb (a and c) and flood (b and d). (a) and (b) correspond to 01 November, (c) and (d) to 11 November. Colours illustrate gradients in sea level.

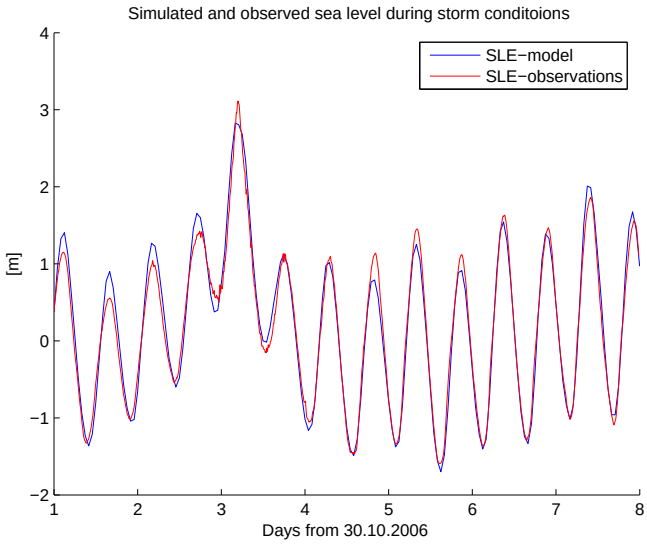

Figure 5: Simulated (blue line) and observed (red line) sea level elevation (SLE) at data station in Otzumer Balje (see Fig. 1 for the location) during storm conditions.

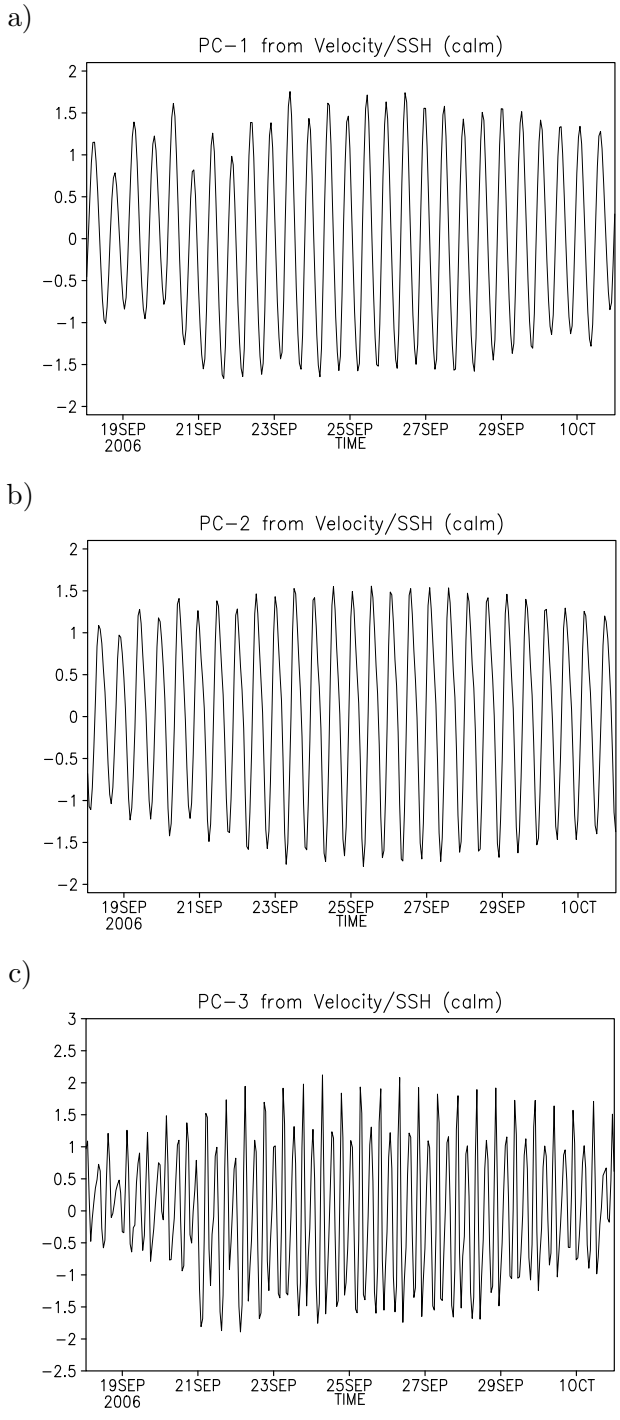

Figure 6: The first three PC-s in "calm" corresponding to dynamical variables (sea level and velocity).

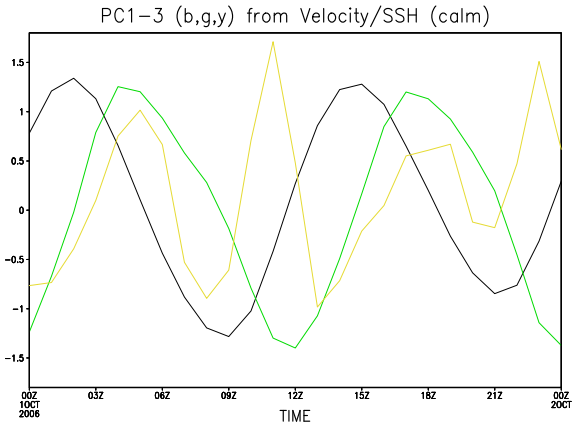

Figure 7: Time-zoom in the first three PC-s, black (PC-1), green (PC-2) and yellow (PC-3) of sea level and velocity.

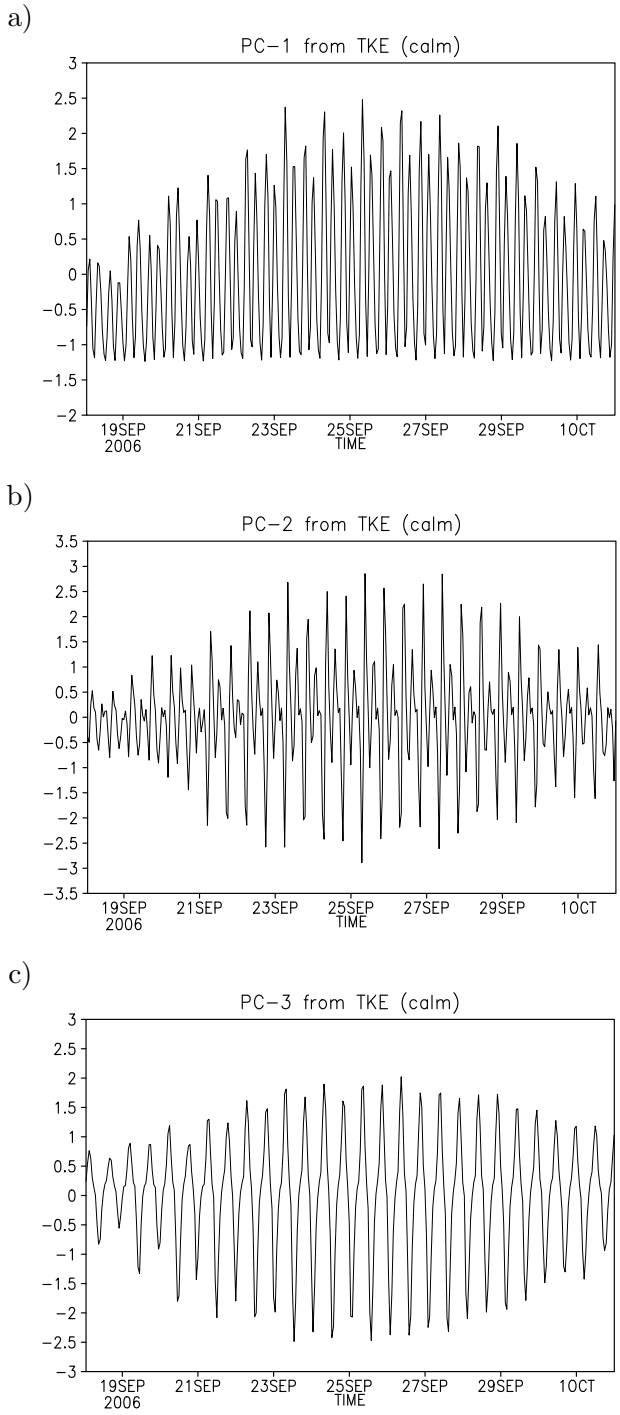

Figure 8: The first three PC-s in "calm" corresponding to TKE.

a)

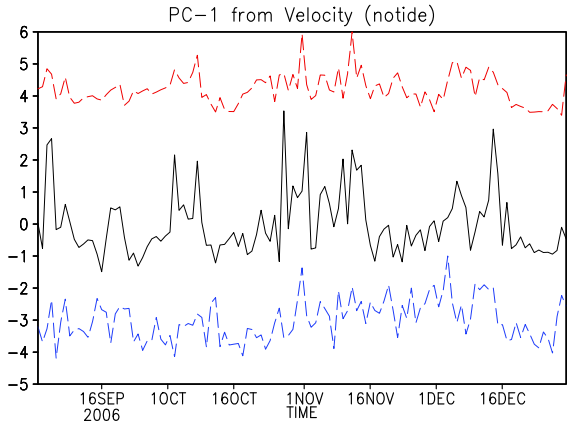

b)

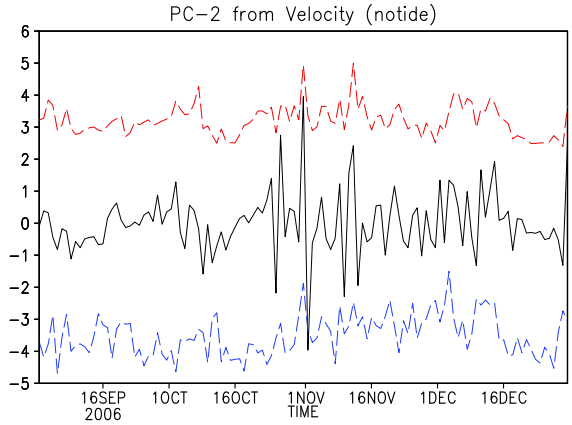

c)

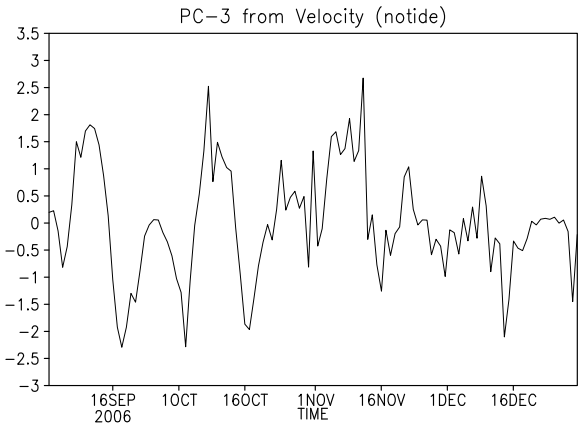

Figure 9: The first three PC-s in "no-tide" corresponding to dynamical variables (sea level and velocity). Dashed lines in (a) and (b) give the course of wind magnitude (blue) and sea level at the open boundary (red) scaled and shifted in order to enable comparison with the PC-s.

a)

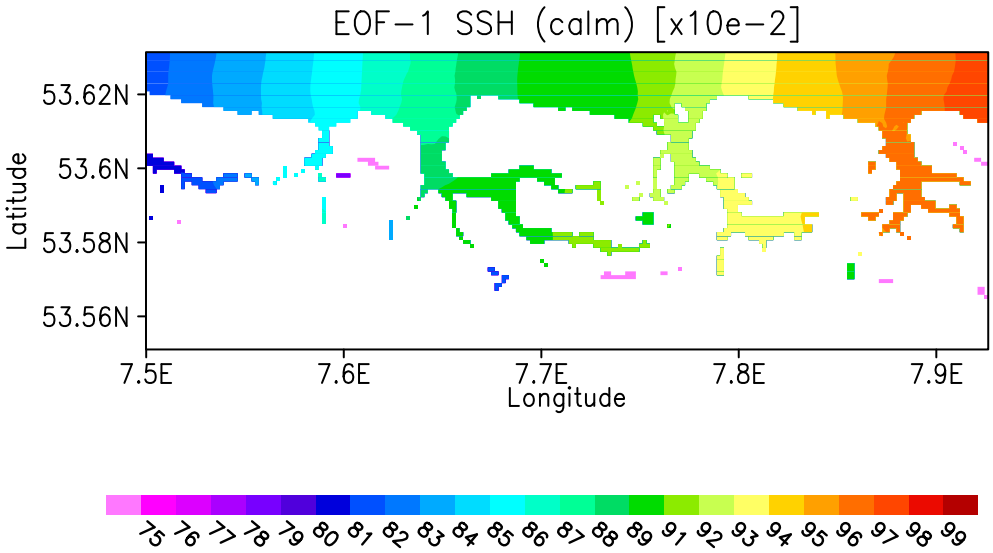

b)

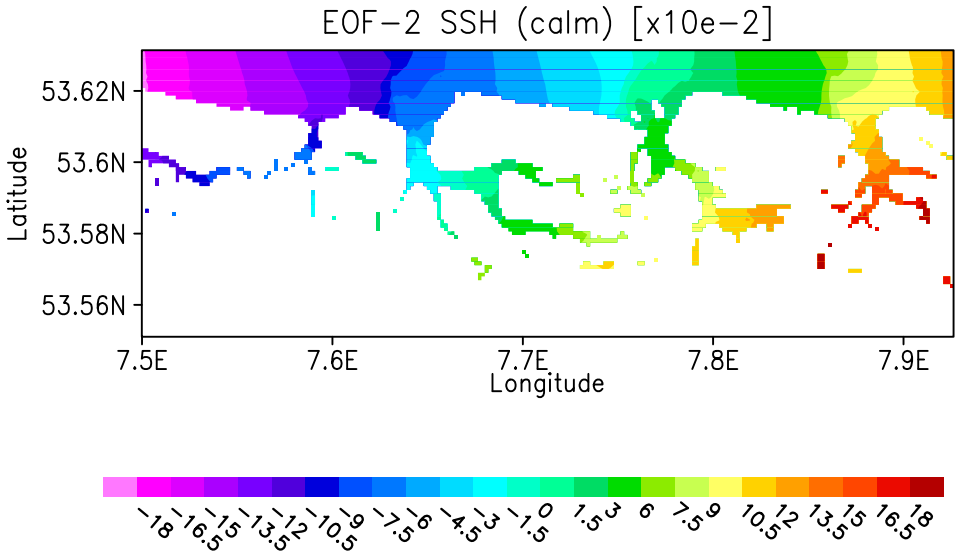

c)

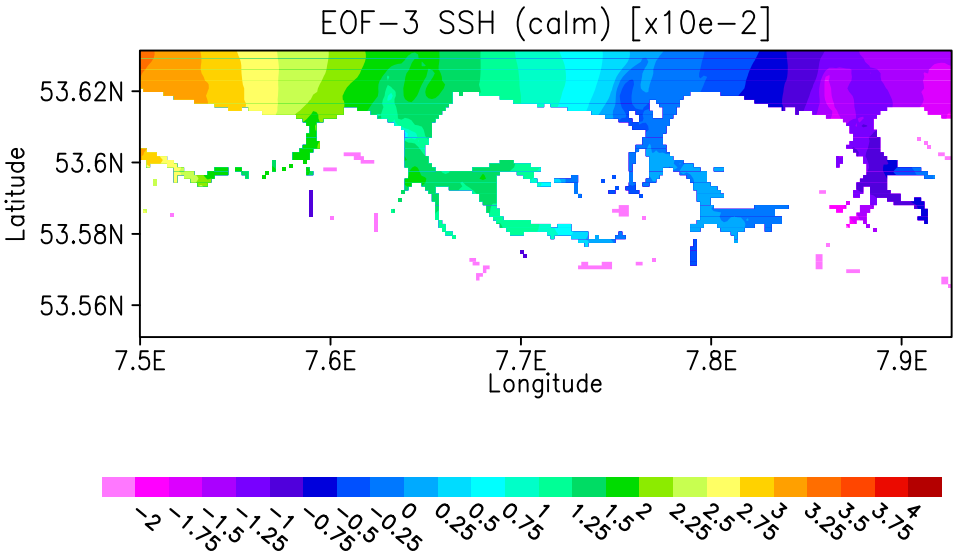

Figure 10: The first three SSH EOF-s in "calm"

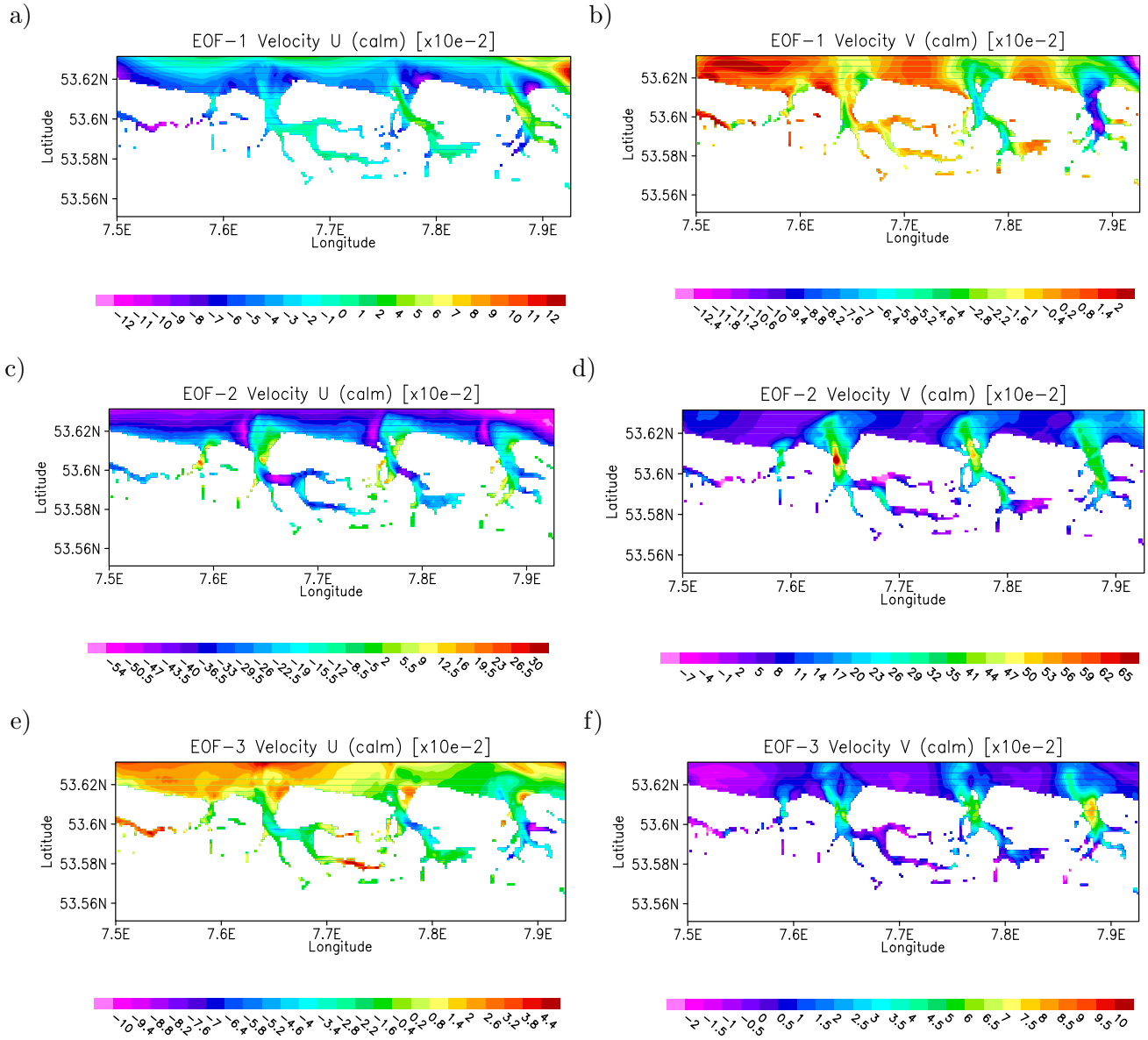

Figure 11: The first three velocity EOF-s in "calm", left: U, right: V.

a)

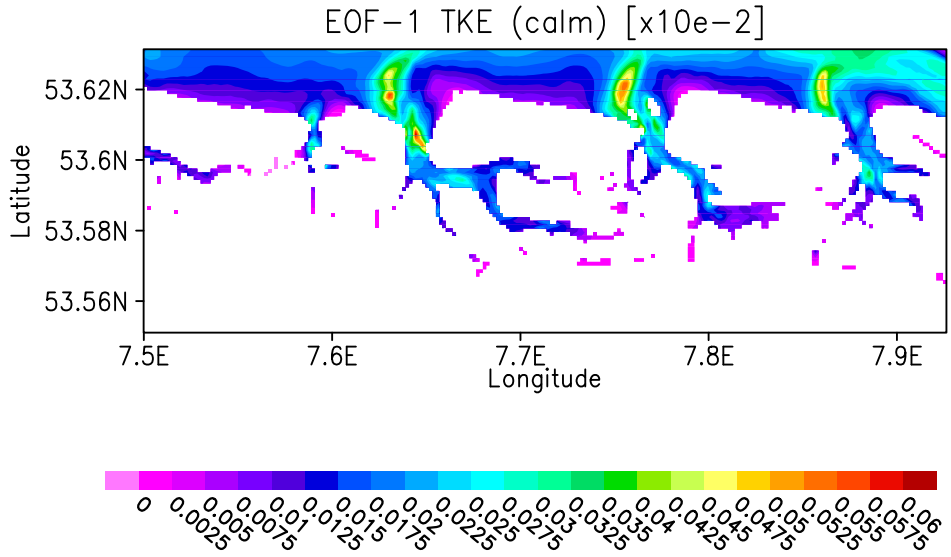

b)

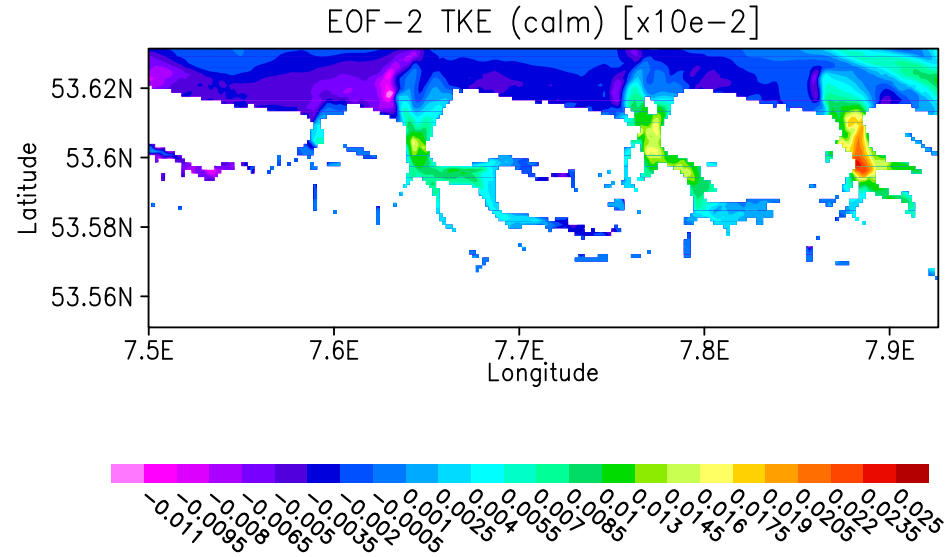

c)

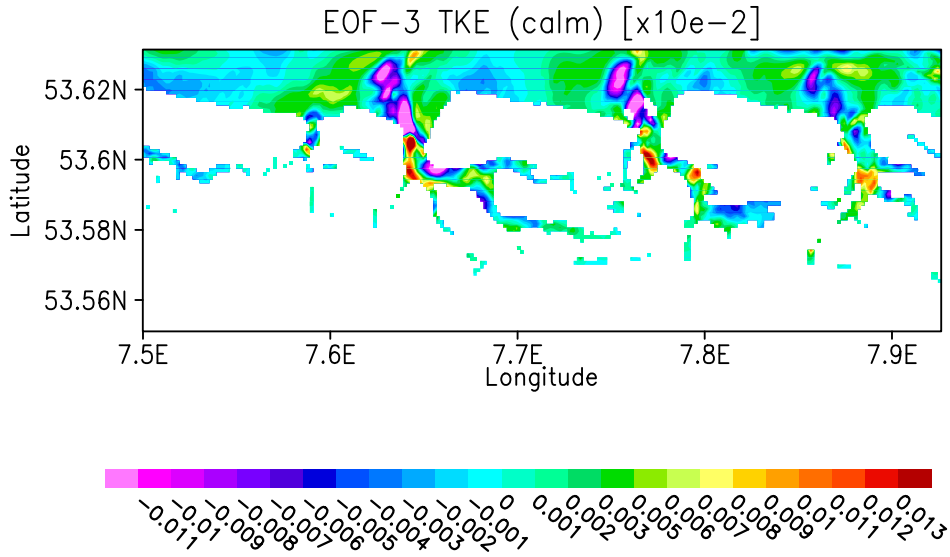

Figure 12: The first three TKE EOF-s in "calm"

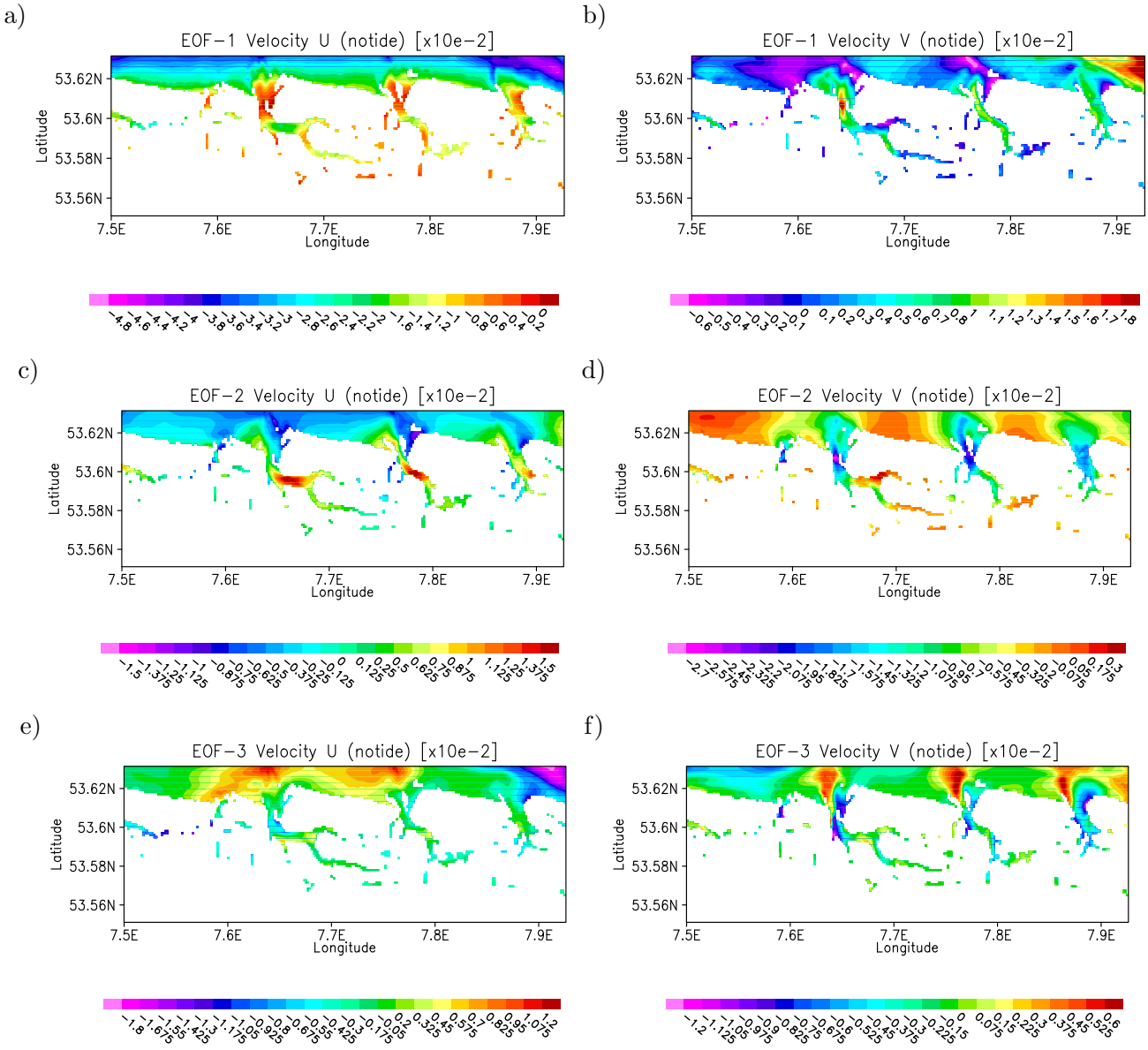

Figure 13: The first three U-velocity EOF-s in "notide", left: U, right: V.

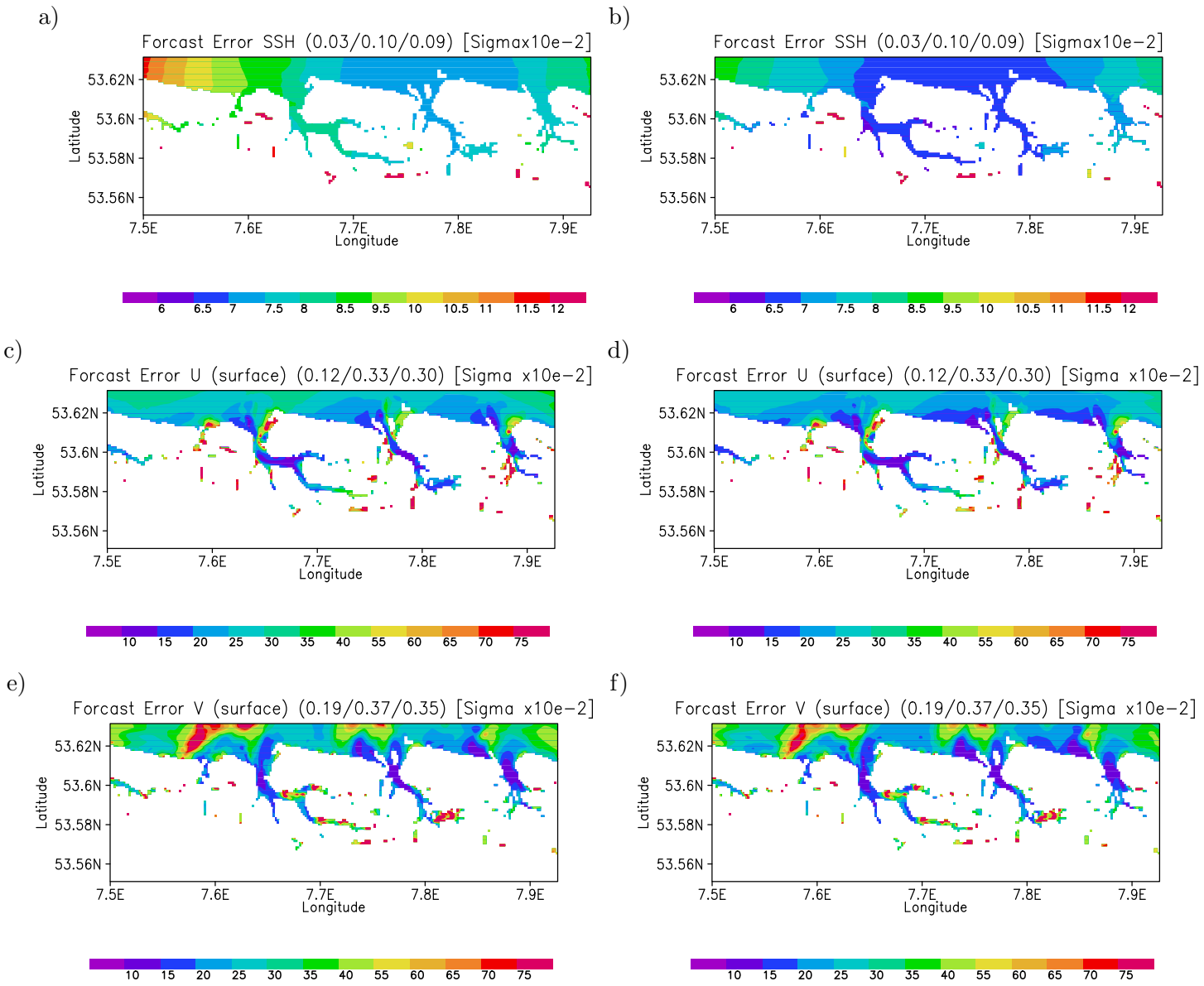

Figure 14: Forecast error for sea level (a, b), u-velocity (c, d), and v-velocity (e, f). Left column: based on one data station, right column: based on two data stations.